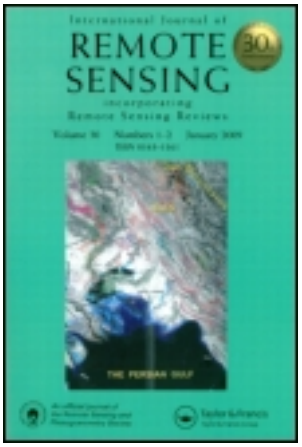

International Journal of Remote Sensing

Publication details, including instructions for authors and subscription information:
http://www.tandfonline.com/loi/tres20

Remote sensing of the 1998 mudflow at Casita volcano, Nicaragua

N. Kerle [a], J.-L. Froger [b], C. Oppenheimer [a] & B. Van Wyk De Vries [b]

[a] Department of Geography, Volcano Remote Sensing Group, University of Cambridge, Cambridge CB2 3EN, UK

[b] Magmas et Volcans (UMR 6524), OPGC Université, Blaise Pascal, Clermont-Ferrand, France

Version of record first published: 27 May 2010

To cite this article: N. Kerle , J.-L. Froger, C. Oppenheimer & B. Van Wyk De Vries (2003): Remote sensing of the 1998 mudflow at Casita volcano, Nicaragua , International Journal of Remote Sensing, 24:23, 4791-4816

To link to this article: http://dx.doi.org/10.1080/0143116031000068187

INT. J. REMOTE SENSING, 10 DECEMBER, 2003,
VOL. 24, NO. 23, 4791–4816

Taylor & Francis
Taylor & Francis Group

Remote sensing of the 1998 mudflow at Casita volcano, Nicaragua

N. KERLE†*, J.-L. FROGER‡, C. OPPENHEIMER† and
B. VAN WYK DE VRIES‡

†Department of Geography, Volcano Remote Sensing Group, University of Cambridge, Cambridge CB2 3EN, UK
‡Magmas et Volcans (UMR 6524), OPGC Université, Blaise Pascal, Clermont-Ferrand, France

(*Received 20 October 2001; in final form 31 October 2002*)

Abstract. A devastating lahar (volcanic mudflow) occurred at Casita volcano (Nicaragua) in 1998, triggered by excessive precipitation associated with Hurricane Mitch. We investigate here the morphology and drainage structure of the flow deposition area, primarily using satellite optical and radar imagery. Because the lahar destroyed several towns and villages, killing over 2500 people, we also assess the utility of images available at the time of the event for disaster management. We find that SPOT multispectral data are most suited to delineate and characterize the flow field, but show limitations for damage assessment, and problems with cloud contamination. ERS Synthetic Aperture Radar (SAR) imagery largely failed to detect the lahar deposits, with RADARSAT performing slightly better. The relatively coarse-grained deposits, together with a dense cover of wooden debris, made the flow nearly imperceptible to the short wavelength C-Band radar, especially at ERS's steep incident angle.

Because of spatial, spectral and radiometric limitations in all types of imagery used, the synergistic potential of optical and radar, as well as high- and low-resolution optical data was explored. The best synergy was found not in merged imagery, but in the incorporation of auxiliary information, such as elevation, map and GIS data. Given the cloud problem, forthcoming radar satellites with variable polarization and incident angles are expected to provide better results in comparable, future situations.

1. Introduction

Following a succession of devastating lahars (e.g. subsequent to eruptions of Mount St Helens (1980), Nevado del Ruiz (1985) and Pinatubo (1991)), the most recent mudflow disaster occurred at Casita volcano, Nicaragua. Excessive rainfall associated with Hurricane Mitch in October 1998 led to a lahar that covered an area of approximately 12 km^2, completely destroying two towns, and killing more than 2500 people (Sheridan *et al.* 1999, Kerle and van Wyk de Vries 2001). The event occurred unheralded, and received a lethargic response. Nicaraguan soldiers only arrived at the scene more than 2 days after the disaster. This resulted from

*Present address: ITC, Hengelosestraat 99, P.O. Box 6, 7500 AA Enschede, The Netherlands; e-mail: kerle@it.nl

International Journal of Remote Sensing
ISSN 0143-1161 print/ISSN 1366-5901 online © 2003 Taylor & Francis Ltd
http://www.tandf.co.uk/journals
DOI: 10.1080/0143116031000068187

(i) officials in Managua questioning reports coming from Casita, (ii) lack of accurate information, (iii) thinly stretched resources due to the widespread effects of the Hurricane, and (iv) impeded access to the site, as several bridges along the main Pan-American Highway had been destroyed, some by Mitch itself.

Timely, reliable and comprehensive information on an event is critical for swift and effective disaster response. Lahars typically cover wide areas or travel long distances, making systematic ground-based information collection all but impossible (Zimmerman 1991, Luscombe and Hassan 1993). Remote sensing technology has been identified as a valuable tool in all aspects of disaster research, including hazard assessment, early warning, syn-event monitoring and recovery (Alexander 1991, Francis 1994, Walter 1994). However, to be effective, imagery must be acquired, processed and disseminated to disaster managers in near-real time, as its information value diminishes exponentially from the time of the event (San Miguel-Ayanz *et al*. 2000). Several researchers have concluded that existing commercial and governmental Earth observation satellites are incapable of a timely response, and have called for satellite constellations solely dedicated to mitigating natural hazard and managing disasters (e.g. Iglseder *et al*. 1995, Kuroda *et al*. 1997, Tobias *et al*. 2000). For a review of the role of remote sensing as a useful tool in lahar disaster response, as well as the need for such dedicated systems, see Kerle and Oppenheimer (2002).

The main aim of this study is to assess the capability of different air- and space-borne systems to delineate and characterize the 1998 Casita lahar deposits. We further evaluate the suitability of the images available at the time of the disaster to provide the critically needed information, above all on the extent of the flow, number of people likely to be affected, and damage to infrastructure (including access), but also on the precise nature of the event, source of the flow, and the potential of further events and remobilization of deposits. We explore combinations of radar and optical data, multi-date composites, as well as integration of elevation, map and GIS data. Lastly, we assess the potential of scheduled and proposed sensors.

2. The Casita lahar seen from the ground

When Hurricane Mitch moved over Central America in October 1998, it generated its maximum rainfall over north-western Nicaragua (Ferraro *et al*. 1999), the location of inactive Casita volcano (figure 1). More than 1200 mm of rain were recorded at the nearest weather station (Chinandega) over the course of 3 days, while the average October rainfall is only 328 mm. Between 10:30 and 11:00 a.m. on 30 October, this excessive precipitation triggered a collapse along Casita's flank, some 250 m south-west, and 100 m below the summit. Approximately $1.6 \times 10^6\,m^3$ of hydrothermally altered and highly fractured rock broke off (Kerle 2002). The resulting debris avalanche quickly transformed into a hyperconcentrated flow, releasing the infiltrated water, which accounted for at least 18% of the collapse volume (Scott *et al*., forthcoming). Aided by a slope angle of about 18°, within 2.5 km of the source, the highly energetic flow had entrained enough sediment to turn into a debris flow, or lahar. The flow had widened to more than 1 km when it arrived, as a 3–5 m high wave, at the towns of El Porvenir and Rolando Rodriguez, located some 6 km south of the summit. Both towns were destroyed beyond recognition. With deposition gradually increasing, by kilometre 10, the flow, now over 2 km

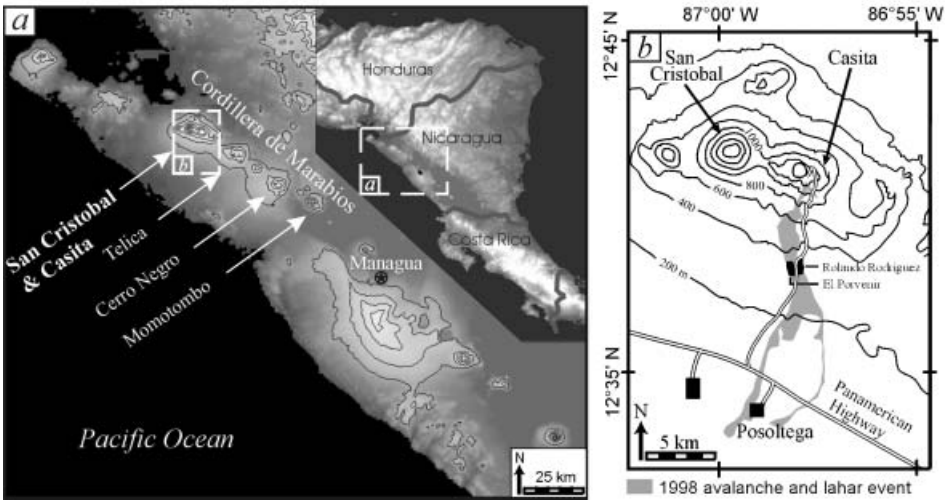

Figure 1. Map showing (*a*) the location of the San Cristobal complex and Casita volcano (elevation 1405 m above mean sea level) within the Cordillera de Marabios; and (*b*) the extent of the 1998 debris avalanche and lahar event (the location of the destroyed towns, El Porvenir and Rolando Rodriguez, is indicated).

wide, entered pre-existing channels and then continued for another 25 km towards the Pacific as a sediment-rich streamflow, still having enough energy to destroy several bridges along the Panamerican Highway.

The deposition surface left by the flow in its various types of transformation is highly variable, ranging from cobble- and boulder-supported avalanche deposits, to pebbly clasts in a muddy matrix in the lahar zone, and finally to smooth, muddy deposits with few clasts in the distal runout area. For further details on the events (including eyewitness reports), and a detailed sedimentological discussion see Kerle and van Wyk de Vries (2001) and Scott *et al.* (forthcoming).

3. Data sources

The analysis presented here is primarily based on space-borne high and low spatial resolution optical, and radar, imagery. A digital elevation model (DEM) was derived from aerial photographs using digital photogrammetry. Table 1 summarizes the datasets we acquired (recall that the event occurred on 30 October 1998).

4. Previous applications of remote sensing for investigating lahars

Showalter and Ramspott (1999; see also Showalter 2001) recently reviewed the use of remote sensing in hazard and disaster research between 1972 and 1998. One principal finding was that remote sensing methods are primarily used for the detection or mapping of hazards and their disastrous effects, but that more complex investigations are rare. This observation holds true for lahar research as well. Table 2 summarizes studies where lahar events were investigated with air- and space-borne imagery. Most papers were concerned with simple delineation of lahar boundaries, either with a single image or in a time-series approach to document change. Two studies (Koopmans and Forero 1993, Carn 1999) further succeeded in discriminating old from recent lahars deposits. Chorowicz *et al.* (1997) had limited

Table 1. Summary of datasets acquired for this study.

Data type	Acquisition date (days after event†)	Track/frame; *Orbit/ID*
SPOT HRV (multispectral, XS)	4 July 1998 (SPOT-3)	616/325
	16 November 1998 (SPOT-4) (17 days)	617/325
	25 November 1998 (SPOT-3) (26 days)	617/325
SPOT-ortho (panchromatic)	1997	n.a. (mosaic of several images)
RADARSAT SAR	3 November 1998 (4 days)	15 648/C0011459
ERS-2 SAR	3 July 1998	348/243; *16735*
	7 August 1998	348/243; *17236*
	11 September 1998	348/243; *17737*
	20 November 1998 (21 days)	348/243; *18739*
AVHRR LAC	various images between June and December 1998	n.a.
Aerial photos	14 January 1996 (1:40 000)	n.a.
	4 December 1998 (1:65 000) (35 days)	
	4 January 2000 (1:40 000) (431 days)	

†For post-event images.
n.a., not applicable.

success mapping actively flowing Pinatubo lahars with radar imagery, finding them too similar to other rough surfaces. Several studies combined different types of imagery, either adding high resolution airborne data to aid interpretation of satellite imagery (e.g. Torres *et al.* 1999), or combining radar with optical imagery (Koopmans and Forero 1993, Garcia *et al.* 1997). One particularly useful mapping approach involved radar-based, multi-temporal colour images to map landscape changes caused by lahars. Pinatubo's smooth-surfaced lahar deposits, generated largely from eroded ash, were especially suitable for images of change produced with short-wavelength ERS Synthetic Aperture Radar (SAR) intensity data (e.g. Chorowicz *et al.* 1997, Torres *et al.* 1999). Table 2 reflects the potential and promise scientists have come to associate with radar data. This is because radar complements optical imagery, and also due to its all-weather, day-and-night imaging capability.

5. Research aims

The aim of this study is to go beyond the identification of the Casita lahar deposit in different types of imagery, and to provide a detailed characterization of the event in light of the following questions:

1. Can we delineate the deposits accurately, and identify the nature of the event?
2. To what extent can we characterize overall structure, surface morphology and sedimentology of the lahar deposits?
3. How accurately can we determine damage to life and infrastructure?

Table 2. Summary of previous remote sensing-based studies of lahars.

Location	Aim	Image type	Techniques	Reference
Nevado Sebancaya (Colombia)	Lahar detection	SPOT XS and Pan (five-image time-series)	Visual analysis	Chorowicz *et al.* 1992
Nevado del Ruiz (Colombia)	Delineation and mapping of lahars (amongst other eruptive products)	SPOT XS	Supervised classification; PCA; ratios	Vandemeulebrouck *et al.* 1993
Nevado del Ruiz (Colombia)	Differentiation between old and recent lahars, including fans built by lahars	Landsat MSS; airborne SAR	Integration of radar intensity with MSS texture and pattern information	Koopmans and Forero 1993
Pinatubo (Philippines)	Lahar delineation	Landsat TM	Visual analysis	Arlene *et al.* 1995
Pinatubo (Philippines)	Lahar delineation	SIR-C	Data acquisition with different polarization combinations, C- and L-Band; clear lahar delineation with L-Band and HV polarization	Mouginis-Mark 1995
Pinatubo (Philippines)	Mapping of temporal and spatial lahar development; relative age dating	SPOT XS; ERS-1 SAR	Visual analysis; stereopair of SPOT panchromatic images	Garcia *et al.* 1997
Pinatubo (Philippines)	Identification of active lahars	ERS-1 SAR	Delineation based on soil roughness, moisture and morphology; multi-temporal colour images to highlight changes	Chorowicz *et al.* 1997

Table 2. (*Continued*).

Location	Aim	Image type	Techniques	Reference
Pinatubo (Philippines)	Mapping of temporal changes in the lahar landscape	Landsat TM; SPOT XS; ERS-1 SAR; SIR-C/X-SAR	Multi-temporal colour images; lahar boundary delineation using filtering, ratios, thresholding; merging of ERS-1 with Landsat TM and Adeos AVNIR images, as well as pre-eruption SPOT XS and post-eruption Landsat TM	Lopez *et al.* 1998a,b
East Java (Indonesia)	Detection and delineation of recent and old lahars at Semeru volcano (as old as 1913)	JERS-1 SAR	Visual mapping; also correlation with fieldwork data	Carn 1999
Pinatubo (Philippines)	Mapping of temporal changes in the lahar landscape	SIR-C SAR; ERS SAR; AIRSAR (POLSAR and TOPSAR)	SIR-C: PCA; density slicing to highlight deposition changes AIRSAR: conversion to decibels; Lee filtering; slant- to ground-range conversion ERS: band-ratio and multi-temporal colour images	Torres *et al.* 1999
Merapi (Indonesia)	Lahar delineation†	SPOT XS	Stereo-SPOT analysis	Thouret *et al.* 2000

†Small aspect of a large hazard-mapping project.

4. How useful is a synergistic integration of radar and optical data, as well as high and low spatial resolution data?
5. How valuable is the integration of elevation, map, and GIS information?

Questions 1–3 are addressed in turn for (i) low spatial resolution optical, (ii) high spatial resolution optical, and (iii) radar data, followed by a separate section on questions 4 and 5.

6. The event seen from space

6.1. *Optical information–low spatial resolution (AVHRR)*

The only type of potentially useful satellite imagery available immediately after the Casita disaster was acquired by NOAA's Advanced Very High Resolution Radiometer (AVHRR), a low spatial (1.1 km at nadir), high temporal (daily) resolution sensor. However, despite daily global coverage, problems related to the satellite's orbit and viewing geometry exist. The large swath-width of 2399 km results in considerable geometric distortion and reduced spatial resolution away from nadir. Furthermore, variable equatorial crossing times lead to occasional night-time imaging, as well as variable solar illumination. Despite extensive coverage of the Casita area following the disaster, the first usable daytime image of the volcano was only captured on 5 November, almost 1 week after the event.

6.1.1. *Delineation*

The chief obstacle in the use of optical imagery in tropical latitudes is cloud coverage. Although Hurricane Mitch dissipated rapidly following the Casita event, the region remained cloudy (figure 2). No AVHRR image until 13 November allows any useful lahar inventory.

Given the limited size of the flow deposit area, AVHRR cannot be expected to provide great detail. The flow can be seen in the 13 November image (figure 3(*a*)).

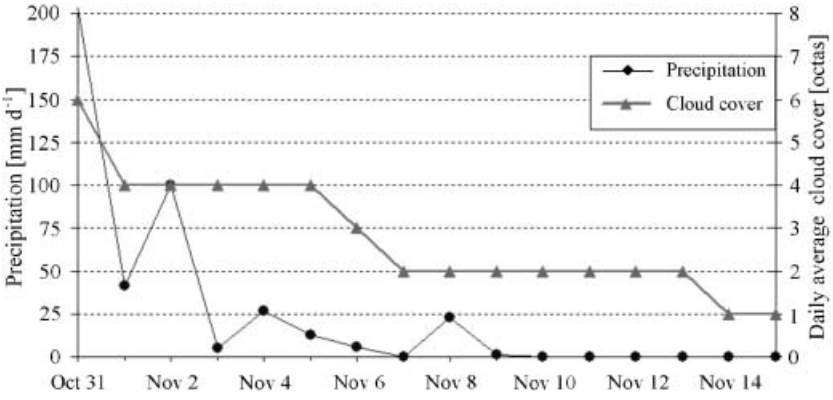

Figure 2. Daily precipitation and cloud cover at the Chinandega weather station after the passing of Hurricane Mitch. Precipitation data are accumulated values recorded at 7 a.m. for the past 24 h. Cloud cover data are in octas (maximum of eight), and correspond to the daily average. Note that the weather station is located approximately 20 km west of Casita, at an elevation of 60 m above mean sea level. Cloud cover is generally higher and more persistent around volcanic structures, as is illustrated by figure 4(*a*).

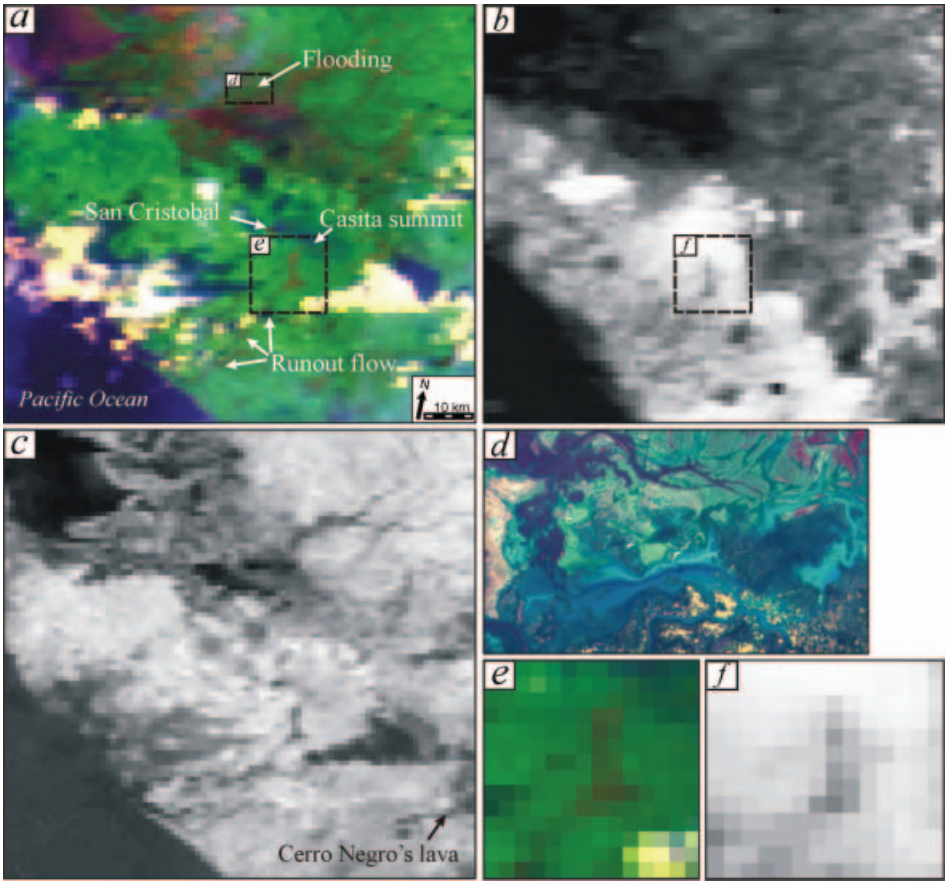

Figure 3. (*a*) False-colour AVHRR composite acquired on 13 November 1998 (bands 1, 2 and 4 as R, G and B, respectively), showing the Casita lahar deposits (subset as (*e*)) and the apparent runout towards the Pacific, as well as spectrally similar flooding (subset of SPOT image of the same area as (*d*)). (*b*) Night-time AVHRR scene of 11 December 1998, showing the deposit's different thermal characteristics (channel 4; subset as (*f*)). (*c*) NDVI image of the 13 November AVHRR scene.

However, it is unlikely that an analyst without detailed knowledge of the area or without auxiliary information would have been able to identify the debris avalanche and lahar as such. This results from (i) the small size of the affected area in relation to the pixel size, (ii) noise introduced by remaining clouds, (iii) mixed pixels, which dilute the signal of the flow deposits, and (iv) the apparent spectral similarity of the lahar deposits to areas merely flooded by sediment-rich river overflow. Several comparatively benign flood areas, which are readily identified as such in the SPOT image, appear spectrally similar to, and even more extensive, than the devastating Casita flow in AVHRR (see §6.2; figure 3(*d*)). Due to the >1 km spatial resolution, image analysis concepts such as site and association, whereby objects are recognized and identified in light of their geographic location and their relation to other features, are only of limited use. Casita cannot be identified as a volcano, nor can rivers be mapped, making the lahar a feature entirely unconnected with its environment.

Sheng *et al.* (1998) used an AVHRR channel 2/channel 1 ratio to detect

large-scale flooding beneath semi-transparent clouds. As this approach relies on the low near-infrared emissivity of water, it is not useful for the detection of freshly drained, moist soil, which emits at similar levels in channels 1 and 2. Therefore, even with available cloud-free AVHRR images, without additional information (high resolution reference/pre-event imagery or local knowledge), a flow event similar in size to the Casita event is unlikely to be detected during a general assessment of a larger area. Simply using a cloud-free pre-disaster AVHRR scene as baseline data is also of limited use. Given the aforementioned variability of illumination and satellite path, a precise pixel-to-pixel registration is impractical, undermining the value of images of change. This problem is exacerbated by the pixel resampling required in such a registration.

After sunset, a strip of denuded land can be expected to display a thermal inertia different from that of vegetated land. Barren lahar deposits would heat up more strongly during the day than areas of dense vegetation, and would appear darker (warmer) in AVHRR's thermal channels (e.g. channel 4; 10.3–11.3 μm). At Casita, the first cloud-free, near-nadir night-time image (taken at 6:43 p.m., just after sundown) is only available for 11 December, about 6 weeks after the event. This is a result of high nocturnal humidity, which leads to recurring cloud cover. The flow is visible in the thermal channel (figure 3(*b*)), and even shows a gradation of grey levels, from brighter at the top of the flow, to darker in the runout area. Reasons for that could be the difference in altitude and ambient temperatures, or a reduced width of the flow towards the source, reducing the size of the thermal anomaly that affects the area of pixel integration.

Freshly denuded areas will also appear as an anomaly in Normalized Difference Vegetation Index (NDVI) images, provided they are of sufficient size, and surrounded by vegetated areas. As with a visual comparison of pre- and post-event images, however, even mildly cloud-contaminated NDVI images are difficult to interpret (figure 3(*c*)). Reference images are critical, as a variety of naturally occurring landforms are unvegetated (e.g. Cerro Negro's lavas). As before, analysis of NDVI without auxiliary information is likely to be of limited success.

6.1.2. *Structure*

Given the improbability of a successful lahar identification, further attempts at a structural assessment seem futile. The small number of pixels encompassing the deposits reveal little detail about the flow, other than that it is straight, and apparently of roughly constant width. A yellow-brown line running south-west towards the Pacific suggests a possible runout flow (figure 3(*a*)).

6.1.3. *Damage assessment*

To be mappable with AVHRR, an object must have minimum dimensions of 2×2 pixels (4.84 km^2; Hanke 1991). This limitation prevents infrastructure and settlements from being identified, making direct damage detection impossible. The added value of GIS information in assessing structural damage is explored in §8.

6.2. *Optical information–high spatial resolution (SPOT)*

In addition to the cloud problem discussed above, SPOT's nominal revisit time is much longer (26 days; with three satellites in orbit (one on standby), SPOT can,

theoretically, image any place on Earth once a day, although that requires an expensive pre-empting of the existing image acquisition schedule, which was not done for the Casita event). The first, partially cloudy, post-disaster image was taken on 16 November (day 17), again almost 2 weeks after the event (figure 4(*a*)). Even if images had been available earlier, they likely would have been cloudy (figure 2). A cloud-free image was taken on 25 November (day 26; figure 4(*b*)). On 20 November (day 21), the first post-event Landsat TM image was captured. Because of partial cloud cover we did not acquire this scene.

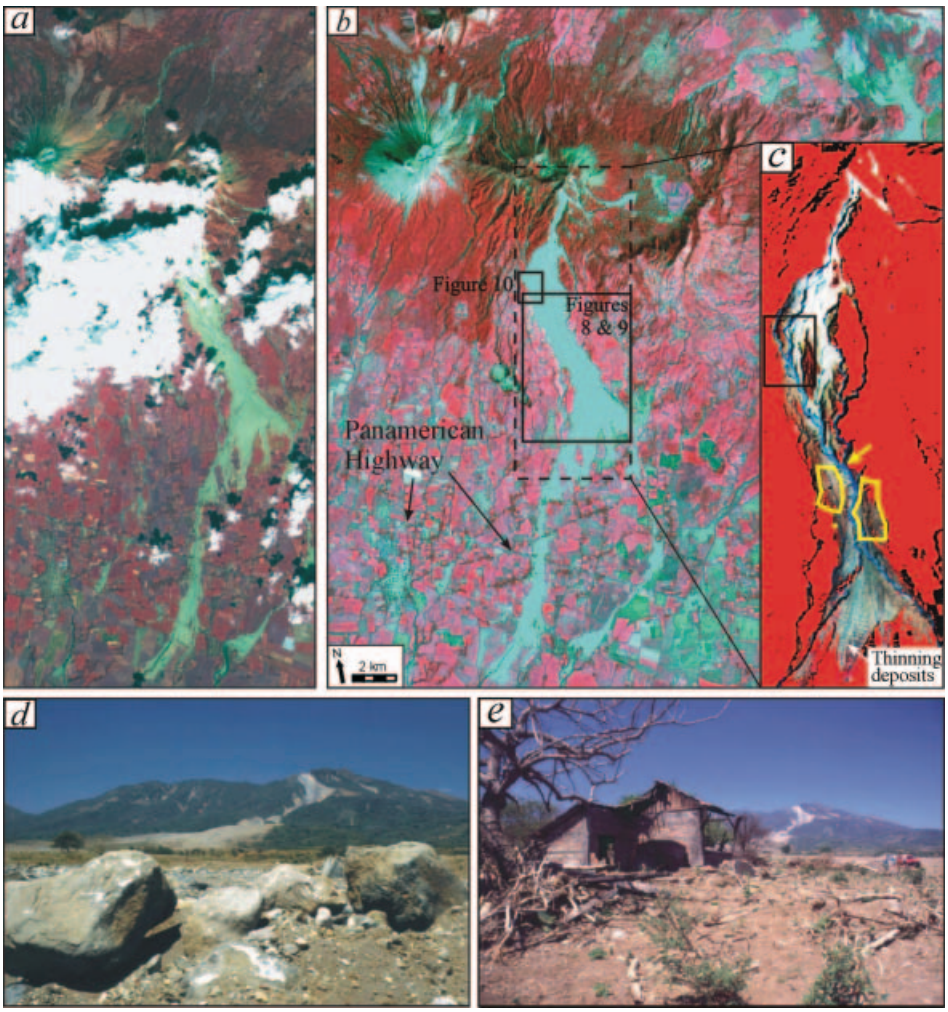

Figure 4. (*a*) SPOT-4 XS subscene of the 1998 Casita avalanche event (bands 3, 2 and 1 as R, G and B, respectively), acquired on 16 November 1998. (*b*) Cloud-free SPOT-3 XS scene of 25 November 1998, and (*c*) contrast-stretched subset. Note the structural detail within the deposit area, including two central channels, which converge just north of the destroyed towns (outlined in yellow), and subsequently bifurcate again. The converged channel had the highest energy and carried large boulders ((*d*); arrow in (*c*) shows location of photo). Only a single house partially survived the lahar ((*e*); location indicated by yellow dot in (*c*)).

6.2.1. *Delineation*

As with AVHRR imagery, the detrimental effect of clouds is apparent in the 16 November image. The 20 m spatial resolution of SPOT XS imagery allows the lower part of the flow to be mapped accurately, yet the source is obscured. With obvious runout flows directed towards the south-west, the flow direction can be inferred. With cloud-free pre-disaster reference images or large-scale maps, detail contained in the image allows the flow to be associated with Casita.

No speculation or inferences are necessary for the cloud-free SPOT scene. Casita is clearly the source of the flow, which was first conveyed through a narrow channel before spilling into the lowlands, fanning out to a width of more than 1 km. After some 10 km, kinetic energy was reduced to a point where the remaining material followed pre-existing riverbeds. The outline is clear and, if the image is geocoded, the covered area can be calculated as approximately 12 km^2.

The nature of the flow, however, remains somewhat ambiguous. The event could have resulted from crater-lake breach, breakout of an equally ephemeral dammed body of surface water generated by the Hurricane's rain, or a flank collapse. In other words, without additional information, the deposits could be identified as those generated by a diluted hyperconcentrated flow, or a debris avalanche which later drained to form the runout flows seen in the image.

6.2.2. *Structure*

Contrast-stretching of the cloud-free SPOT scene reveals substantial drainage structure within the flow deposits (figure 4(*c*)). It is evident that most of the flow material initially followed a narrow, incised thalweg, likely gaining pace before reaching the faldas, the volcanic alluvial aprons, where it spread out and decelerated. Fieldwork has confirmed the thalweg's slope angle of 18°, with associated flow speeds of 40–70 $m\,s^{-1}$ (K. Scott, personal communication). The AVHRR images had suggested that, following the initial spreading, the flow retained a nearly constant width. The SPOT image, however, reveals a distinct channelling throughout the entire flow, with a considerable narrowing just north of the towns resulting from a convergence of two separate channels (see arrow in figure 4(*c*); towns outlined in yellow). This channel would have had the highest flow energy and, consequently, contained most of the material and larger boulders. This too was confirmed by fieldwork. Most blocks and boulders were conveyed through that channel, some being left behind as energy waned (figure 4(*d*)).

Remote sensing has been used previously to map volcanic debris avalanches (e.g. Francis and Wells 1988, Wadge *et al.* 1995), taking advantage of morphological characteristics such as hummocks, marginal levees, and longitudinal and transverse ridges (Siebert 1984, Ui *et al.* 2000). Such signature features are absent in the SPOT image of the Casita flow. Vallance (2000) also maintained that there is no single morphological feature that allows a differentiation between lahar and avalanche deposits, as lahars too can carry megaclasts and produce levees. Further, the actual debris avalanche deposits (kilometre 0.0 to $\sim$1.2), despite their poor sorting, are also rather fine (mean diameter -4 to $-6\,\varphi$ (16–64 mm); Scott *et al.*, forthcoming), lack hummocks, and are only less than 5 m thick. The channel network, clearly seen in figure 4(*c*), could also be a secondary feature, as debris avalanches are known to become subsequently incised by a new drainage system

(Ui *et al.* 2000). With the SPOT image alone, some ambiguity concerning the precise nature of the flow and its transformation phases remains.

It would be equally misleading to rely on the *H*/*L* ratio, the equivalent coefficient of friction, which expresses the relationship between vertical drop (*H*; for example taken from a map or DEM) and runout distance (*L*) as a measure of mobility. The value for the entire flow, 0.114, precisely matches the median value of various debris avalanches reported by Siebert (1984). The *H*/*L* ratio became a popular indicator following the 1980 Mount St Helens eruption and avalanche, used to investigate the runout behaviour of debris avalanches, lahars and pyroclastic flows (Ui 1983, Siebert 1984). The *H*/*L* relationship, however, tends to be highly irregular, as it strongly depends on topography (such as channelling) in the runout path, and is now less frequently used.

Considering the high velocity of the flow when it reached the towns, the abrupt termination of the main flow is puzzling. There is a distinct transverse striping in the lower end of the deposition field, an indication of thinning sediments that reveal shallow field terracing typical for the region (figure 4(*c*)). Instead of a flow termination, this area appears to be a fan-like, single-wave overspill. It primarily results from (i) bifurcation of the central channel, (ii) energy loss due to the high hydraulic roughness of the towns, and (iii) topographically controlled flow-widening. The sharp lower right edge of the fan area is clearly a result of local blockage (which was breached in two places), which caused the already sediment- and energy-poor overspill to travel further to the south-west. There is no evidence of the fan tapping into either of the principal channels. Despite weakly established radial flow features directed towards the bifurcation, the fan does not appear to have evolved over time, but was likely deposited in a single overspill.

6.2.3. *Damage assessment*

Image-based damage detection relies on an affected object's visibility. The first scientific party to reach the site, about 1 week after the event, could only locate the two towns by GPS (Sheridan *et al.* 1999). Indeed, in the SPOT image there is no trace of settlements within the flow boundaries. However, without knowledge of the towns' existence they would not get classified as destroyed or damaged. This problem is amplified by (i) the small size of the towns, (ii) the widespread use of natural construction materials, and (iii) trees hiding buildings (figure 5(*a*)). It also emerged later, that the combined population only approached 1500, with most of the remaining victims having sought shelter from the torrential rains. Therefore, images analysis alone can lead to wrong conclusions about the number of people affected.

Hanke (1991) stated that, similar to AVHRR, SPOT XS's resolution allows mapping of features as small as 0.16 ha (2×2 pixels). However, in low-contrast images, the minimum object size can increase to 16 ha for object detection, and even 36 ha for object recognition (i.e. identification of the towns as such; Rengers *et al.* 1992). This makes the detection of smaller hamlets, some of which were destroyed as well, even less likely. With such small-sized settlements only a comparison with suitably high-resolution, pre-event imagery (space- or airborne) would reveal their accurate location.

A further problem relates to the central channel identified in the enhanced image. It suggested that a disproportionate amount of material was confined to a narrow width, seemingly just sparing the towns. In fact, the towns are completely

destroyed, and only one house partially survived the flow (figure 4(*e*); yellow dot in 4(*c*) at the western deposit edge indicates position). The image simply does not convey the destructive impact pressures as high as 10^4–10^6 kg m^{-2} produced by lahars (Rodolfo 2000), nor does it reflect the flow's central wave height of 3–5 m when it met the towns (Scott *et al.*, forthcoming). In this case, image analysis can only reveal that the towns (provided their existence was known) were likely damaged, possibly severely as the overall deposit width coincides with the towns' extent, and that an urgent field investigation is necessary.

Damage to the Panamerican Highway is easier to assess, as the road is readily identified, and is clearly intersected by the flow in two places (figure 4(*b*)). Any effect on other important infrastructure, such as power or communication lines, cannot be detected directly, but would require a more detailed analysis within a GIS framework (see §8).

6.3. *Radar information–ERS-2 and RADARSAT*

Our post-disaster ERS-2 image was acquired on 20 November (day 21; incident angle of 23°), the RADARSAT scene on 3 November (day 4; 31–46°). In addition, we obtained three pre-event ERS images taken in July and August 1998 to understand better the normal temporal variability in backscattering, related not to disastrous events but seasonal vegetation change. Both satellites operate in C-Band (5.6 cm wavelength), ERS in VV, RADARSAT in HH polarization. ERS has a repeat time of 35 days, while RADARSAT is steerable, allowing the return time to be reduced to 1–5 days (depending on latitude; nominal revisit time is 24 days). While the ERS images have a 30 m spatial resolution (with four looks) and 16 bit dynamic range, the RADARSAT scene is only a ScanSAR Narrow product with 50 m resolution and 8 bit range.

6.3.1. *Delineation*

For the Casita flow deposits to be apparent in radar imagery, either their roughness (with respect to the signal wavelength) or their moisture (i.e. the surface dielectric constant) must differ from the surroundings. Figure 6(*a*) shows that this is not the case for the ERS image. Except for the distal runout areas (figure 6(*d*)), which are radar-dark, the sensor did not highlight the flow. Clearly, what worked well at Pinatubo (Chorowicz *et al.* 1997, Garcia *et al.* 1997, Lopez *et al.* 1998b) failed at Casita. Had the flow resulted in persistent flooding, it would have shown in the image. However, there were no obstacles along Casita's smooth lower flank that could have led to water retention. None of the survivors interviewed by Barreto (1998) reported any standing water. Therefore, following the initial drainage of the deposits, their moisture would have been similar to that of the surrounding terrain.

Despite the identical wavelength, RADARSAT managed to record the central deposition field (if weakly), as well as the runout areas (figure 6(*e*)). Deconvolving the complex radar signal, which is a function of several terrain characteristics (e.g. surface roughness, local slope) and instrument parameters (e.g. polarization, incident angle) with only a single-band image is not possible, leading to inevitable ambiguities (Dobson *et al.* 1995). A comprehensive assessment of the differences in

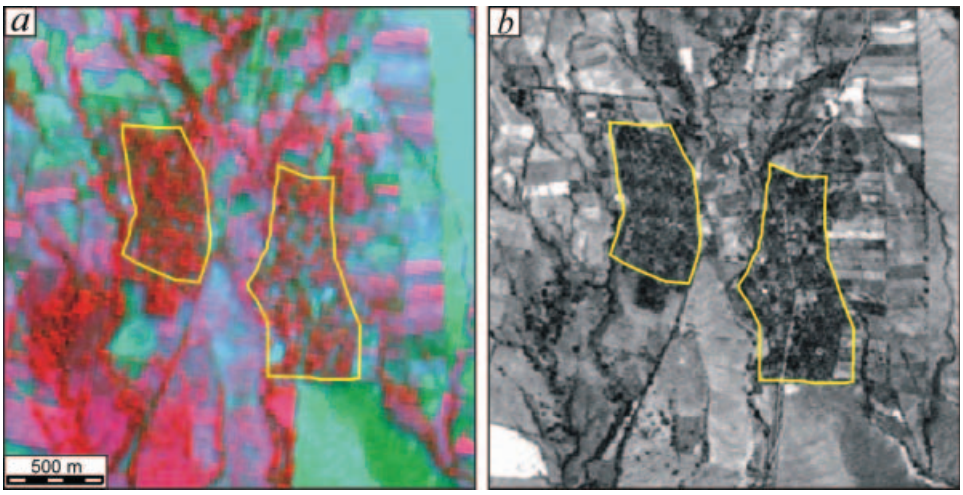

Figure 5. (*a*) Subset of the 4 July 1998 (pre-event) SPOT XS scene illustrating difficulty in recognizing the destroyed towns (outlined) as such. (*b*) Recognition is easier in a panchromatic SPOT image (10 m spatial resolution), yet still largely relies on the distinct shape and roads.

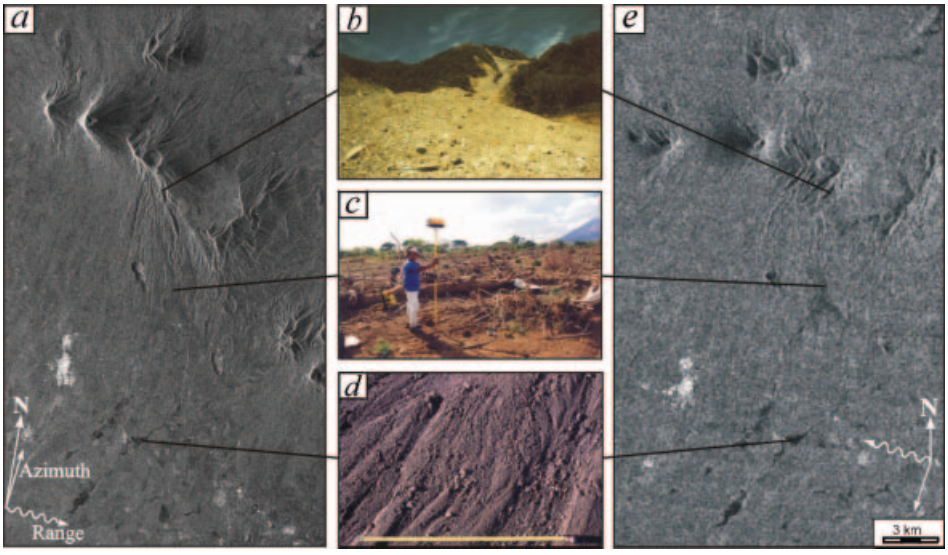

Figure 6. (*a*) Ascending ERS-2 SAR image of Casita and San Cristobal, acquired on 20 November 1998. Incident angle is 23°, with illumination from the west, VV polarization, 30 m spatial resolution. Note that the main deposition field is not readily apparent, but that only the distal runout areas appear radar dark. (*b*)–(*d*) highlight a change in surface roughness, from coarse debris avalanche deposits in the first 2 km (*b*), to smoother lahar deposits (though covered in wooden debris; (*c*)), and smooth, fluvial deposits left by the hyperconcentrated runout flow (*d*). The ruler is approximately 60 cm long. (*e*) A descending RADARSAT ScanSAR Narrow image of the same area, acquired on 2 November 1998. Incident angle is 31–46° with HH polarization, 50 m resolution, and illumination from the east. Note how the main deposit area is more clearly visible than in the ERS image.

backscatter would require quad-polarized and/or multifrequency data. In the Casita images, the difference in grey values between the central and distal areas could reflect a change from coarser to smoother deposits. Alternatively, the main deposit field could also be wet, with a comparatively high dielectric constant resulting in relative brightness, while the runout areas correspond to pools of standing water, and consequently radar-dark specular reflection. However, ground data suggest roughness differences to be responsible. Figure 6(*b*)–(*d*) reveals a transition from coarse avalanche deposits in the upper reaches, including boulders ($> -8\,\varphi$ (256 mm)), to very fine fluvial sediments deposited by the runout flow. The distal runout areas correspond to floodplains, which showed no signs of damming. Precipitation also ceased on 9 November (figure 2). Therefore, at least in the ERS image we can discount moisture as the reason for backscatter variability.

The main difference from Pinatubo is that the Casita lahar resulted largely from disintegrated flank collapse material and colluvium, and not from fine ash. Nevertheless, the lahar deposits consist mostly of fines drained from the debris avalanche, and fine colluvium eroded along the falda, with average particle size decreasing from 5.1 to only 2.0 mm along the course of the lahar (Scott *et al.*, forthcoming). The zone probably appears rough to ERS because it was littered with wooden debris from the forest that was destroyed by the debris avalanche (figure 6(*c*); see also figure 4(*e*)). RADARSAT's ability to image the central deposit field likely results from its higher, more oblique, incident angle. Clearcuts, similarly rough surfaces with tree stumps and slash piles, have previously been identified more successfully with higher incident angles (Yatabe and Leckie 1995).

Using a similar approach to Chorowicz *et al.* (1997) and Lopez *et al.* (1998b) at Pinatubo, we produced a false-colour composite of two terrain-corrected and geocoded ERS scenes, specifically one pre- (11 September), one post-disaster (20 November), and their first principal component (figure 7). Orange hues correspond to a decrease in backscatter intensity, blue ones to an increase. The smooth runout deposits appear orange, but the central part of the flow (outlined) is almost imperceptible. We would expect better results with (i) a longer wavelength (e.g. L-Band; 24 cm), (ii) a similar image constructed from two RADARSAT scenes with higher incident angles, or (iii) cross-polarization, with the latter more successfully highlighting the unaffected, surrounding vegetation. It is difficult to predict, whether like- or cross-polarization will be superior for a given area. However, a study by Guo *et al.* (1997) demonstrated radar's ability to differentiate diverse volcanic surface materials, when different polarizations are available. They showed that for both L- and C-Bands, cross-polarization resulted in greater separability of different materials than like-polarization. Mouginis-Mark (1995) also successfully used cross-polarization (HV) to map Pinatubo's lahars, in addition benefiting from L-Band's longer wavelength. Envisat's Advanced Synthetic Aperture Radar (ASAR) will have variable incident angles and polarizations, and could prove useful for future mapping of young lahar deposits.

We further attempted an interferometric analysis of the flow area, using pre- and post-event ERS images. However, due to the vegetation cover, coherence was lost in between scenes. In less vegetated areas, or with a longer wavelength, fringe patterns could have revealed erosion and deposition areas within the flow zone.

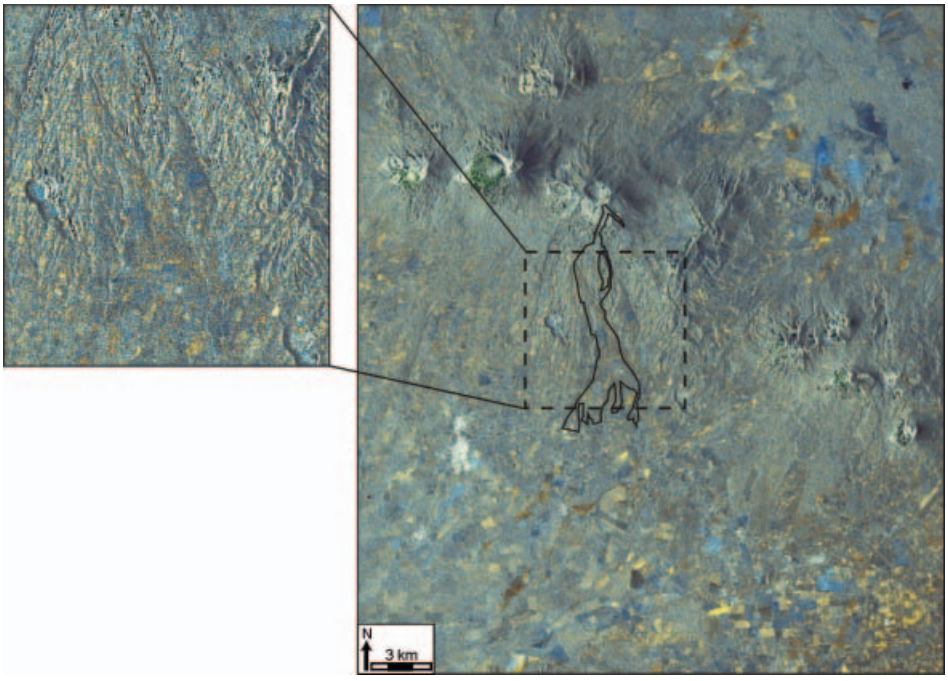

Figure 7. Colour composite of a pre- (11 September) and a post-disaster (20 November) ERS SAR image, and their first principal component. See text for discussion.

6.3.2. *Structure and damage assessment*

With the principal deposit field not appearing in ERS, and only barely in the RADARSAT image, little additional information can be extracted. With previous knowledge of a lahar event in that Casita sector, however, it is possible to infer that no persistent flooding has occurred. Further, had any hummocks, dikes or other lineaments been produced, especially oriented along a north–south axis (perpendicular to the sensor look angle), they would likely have appeared in the imagery (see, for example, Vencatasawmy *et al.* 1998). A single bright line, oriented in this direction, likely corresponds to the narrow valley through which the debris avalanche moved (figure 6(*b*)). The lahar only produced levees 5–20 cm high, not enough to appear in the radar images.

Neither image is very suitable for damage assessment. The towns, camouflaged by trees, were not efficient corner reflectors, and therefore are not visible in the pre-event scenes. It is also not directly apparent that the flow crossed and damaged the highway.

7. Synergistic imagery

Merging complementary information, either spatial or spectral, has the potential to reveal details that may otherwise remain obscure or ambiguous. Similar to the layering structure of a GIS, analysis of one information layer is informed and enhanced by data from another. High synergistic potential lies in the merging of low with high spatial resolution images, and in the combination of optical and microwave datasets. Integration is typically achieved by incorporating a single band or image, for example a radar intensity layer, into a multi-band image transformed

either by principal component analysis (PCA), intensity–hue–saturation (IHS), or high-pass-filter methods. After substitution, the merged image is returned to RGB by inverse transformation (see, for example, Harris *et al*. 1990, Chavez *et al*. 1991). Whenever preservation of the spectral characteristics of the original multispectral image is critical, alternative methods, such as the Price algorithm (Shaban and Dikshit 2001) or wavelets (e.g. Zhou *et al*. 1998) may be more appropriate (see also Pohl and van Genderen 1998).

7.1. *Integration of high and low spatial resolution images*

The spatial resolution of multispectral SPOT imagery was sufficient to delineate and characterize the Casita flow deposits, but of limited use in damage assessment. Therefore, pre-event aerial photographs, with an object space pixel resolution of 0.56 m, were orthorectified and integrated with the multispectral data, using IHS and PCA transformations. Recall that the photos were acquired before the disaster, hence their benefit in the flow structure assessment described above is an indirect one, mainly deriving from surface cover and topographic information. Here they are used to highlight infrastructure that may have been affected by the lahar. Small-scale (1:65 000), monoscopic, post-event photos were acquired as part of the US Open Skies programme in December 1998 (Molnia and Hallam 1999). A comprehensive mission, acquiring photos at a scale of 1:40 000, was only accomplished in January 2000, by which time substantial re-vegetation had occurred in the lahar deposition area, greatly reducing the photos' utility for this study.

Figure 8(*a*)–(*c*) shows the three principal components (PCs) for the area surrounding the destroyed towns, calculated from the cloud-free SPOT image (location of subset indicated in figure 4(*b*)). It is apparent that, with the disappearance of the scene brightness contained in PC1, the deposit outline in the reversed image has faded (figure 9(*a*)). Despite the detail from the photos, it is unclear which areas were affected. Using the enhanced SPOT image (figure 4(*c*)) leads to a different problem: although the deposits are clearly outlined, and the structural features identified earlier can be seen, much of the spatial detail from the photos has disappeared (figure 9(*b*)). This is because the new PC1 (not shown), especially in the area outside the deposition zone, correlates much less with the aerial photos.

Better results were obtained with an IHS transformation of the unstretched SPOT sensor image. Figure 8(*d*)–(*f*) shows intensity, hue and saturation, respectively. Although some of the structural features, contained in the intensity layer, are lost in the reverse transformation, the resulting image (figure 9(*c*)) clearly shows deposit extent and main channels, as well as the towns. As was reported in other studies (e.g. Chavez *et al*. 1991, Zhang 1999), the spectral characteristics of the image were changed during the re-transformation.

Although the spatial resolution of neither PCA- nor IHS-transformed image quite matches that of the integrated panchromatic image (Li 2000), the aerial photos used here show excellent detail. SPOT panchromatic data, with 10 m spatial resolution, would have been a poor alternative, considering the size of the objects of interest. Indeed, even a positive identification of the towns would not be possible without the peculiar shape and the obvious roads (figure 5(*b*)). As before, smaller hamlets cannot be identified.

A useful alternative to image fusion is a separate stereoscopic analysis of the pre-event aerial photos, which, as is common, were acquired in overlapping strips.

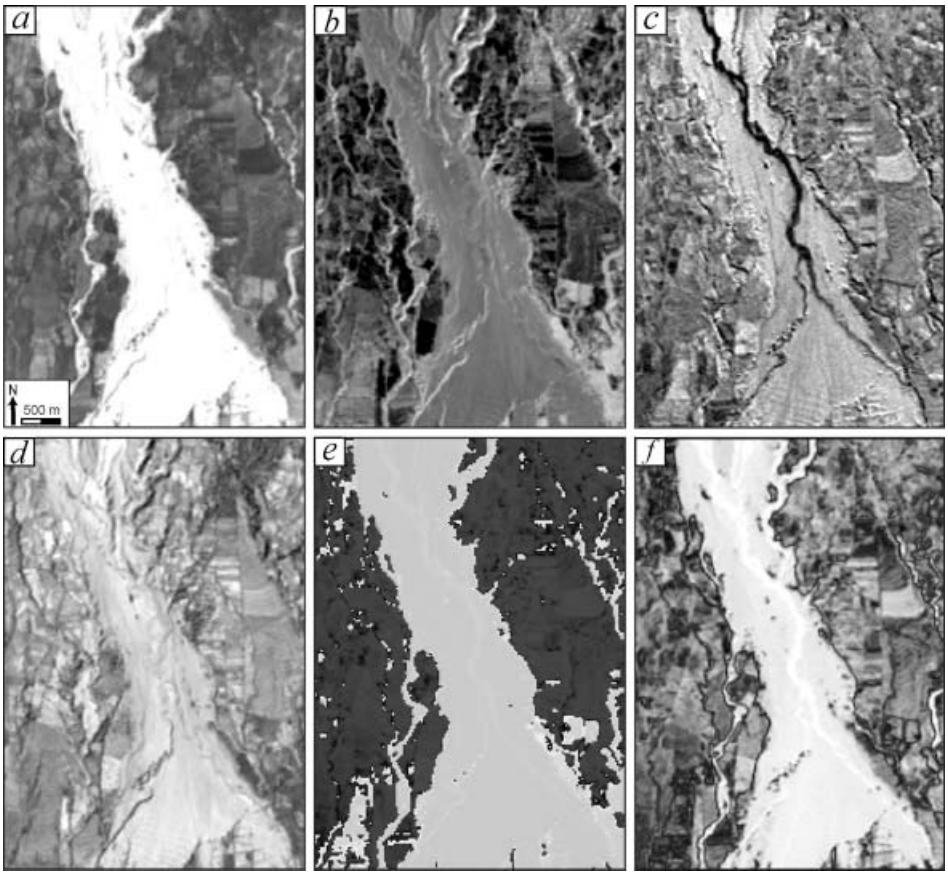

Figure 8. (*a*)–(*c*) Subset of principal components of unstretched SPOT image of 25 November 1998. (*d*)–(*f*) Intensity, hue and saturation images, respectively, of the same scene.

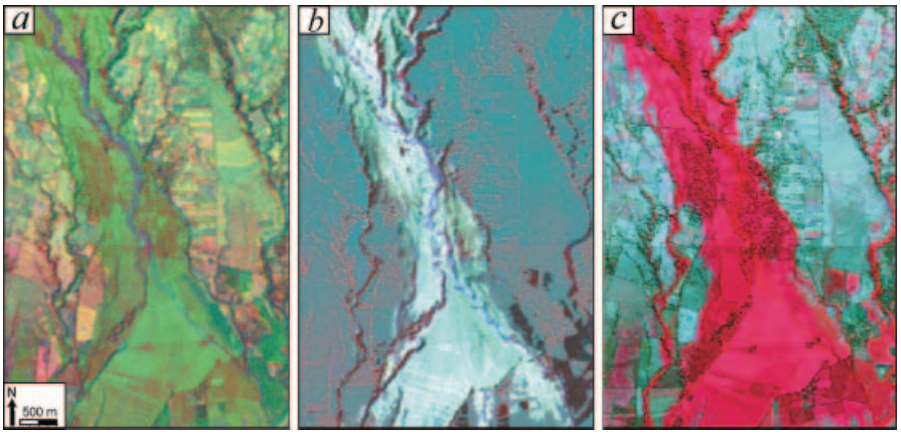

Figure 9. (*a*) Aerial photo from 1996, showing the destroyed towns, substituting PC1 of the unstretched SPOT image (figure 8(*a*)), after inverse principal component computation. (*b*) same as (*a*), but using the PC1 based on the contrast-stretched SPOT image (figure 4(*c*)). (*c*) Aerial photo from 1996, after inverse IHS transformation, replacing the intensity layer. See text for discussion.

Here the images were converted into anaglyphs in ERDAS Imagine's Stereo-Analyst, which allows on-screen quantitative work in geographic space, as well as incorporation of additional vector information, such as image classification results. It is clear that all major channels identified in the SPOT image correspond to pre-existing channels. Although Scott *et al.* (forthcoming) found local channel deepening of up to 2 m in the distal runout area, channels in the upper lahar zone show a surprising lack of widening and change in depth. A detailed DEM-of-change with 0.8 m grid spacing, based on 1996 (figure 10(*a*)–(*b*)) and 2000 (figure 10(*c*)–(*d*)) aerial photos revealed no distinct pattern.

7.2. *Optical and radar information*

Synergy can only be achieved when both elements, two complementary image sources in this case, contribute mutually exclusive information. Neither post–event ERS nor RADARSAT image offers much in this respect. The surface is not dry, nor is the wavelength long enough to allow ground penetration, which could have identified features beneath the deposits. Linear features, such as dikes or levees, would aid in the interpretation of optical data, yet are not apparent. Merging the post–event ERS and SPOT images, however, shows that the narrow lower right runout flow (see figure 4(*b*)) is a deep gully, resulting in a bright return in the radar image (figure 11), while the left runout flow is not.

8. The added benefit of elevation, map and GIS information

All types of imagery used in this study have shown some limitations. In AVHRR imagery, the disaster zone appears to be entirely unconnected with its environment, as, due to the low spatial resolution, neither the volcano nor rivers can be identified. Even the SPOT image with its high spatial resolution could not readily identify damage to infrastructure. Auxiliary spatial information, including DEMs, topographic and thematic maps, and GIS datasets, are becoming increasingly available for many countries, and can easily be combined with remote sensing data. Jiang and Cao (1994) demonstrated the advantage of combining GIS with remote sensing data to assess damage caused by flooding in near real-time. The role of GIS in volcanic risk management and damage assessment at Etna and Vesuvius was investigated by Pareschi *et al.* (2000). One of the aims of NASA's Shuttle Radar Topography Mission in 2000 was the generation of a near-global DEM (60° N–56° S) at 30 m resolution. A 90 m DEM is expected to be available in the public domain (see http://www.jpl.nasa.gov/srtm/dataproducts.html).

The US Federal Emergency Management Agency (FEMA) lists 21 'elements of essential information' for emergency support (Birk *et al.* 1995), many of which, such as administrative boundaries, cannot be discerned directly from satellite imagery. Figure 12(*a*),(b) shows the 13 November 1998 AVHRR image within a GIS framework. Provided the flow feature is recognized as such (e.g. based on actual field reports), the flow direction is given by the contours, pointing to the volcano as the source. River overflow can largely be discounted. Depending on the comprehensiveness of the database, lifelines, settlement locations (and population numbers), and other relevant features can be related to the image. Figure 12(*b*) shows that at least one settlement was affected by the lahar. It is also clear that a provincial boundary lies just east of the flow. A similar political division around Arenal volcano (Costa Rica) led to a serious obstruction of emergency planning (Kerle 1996).

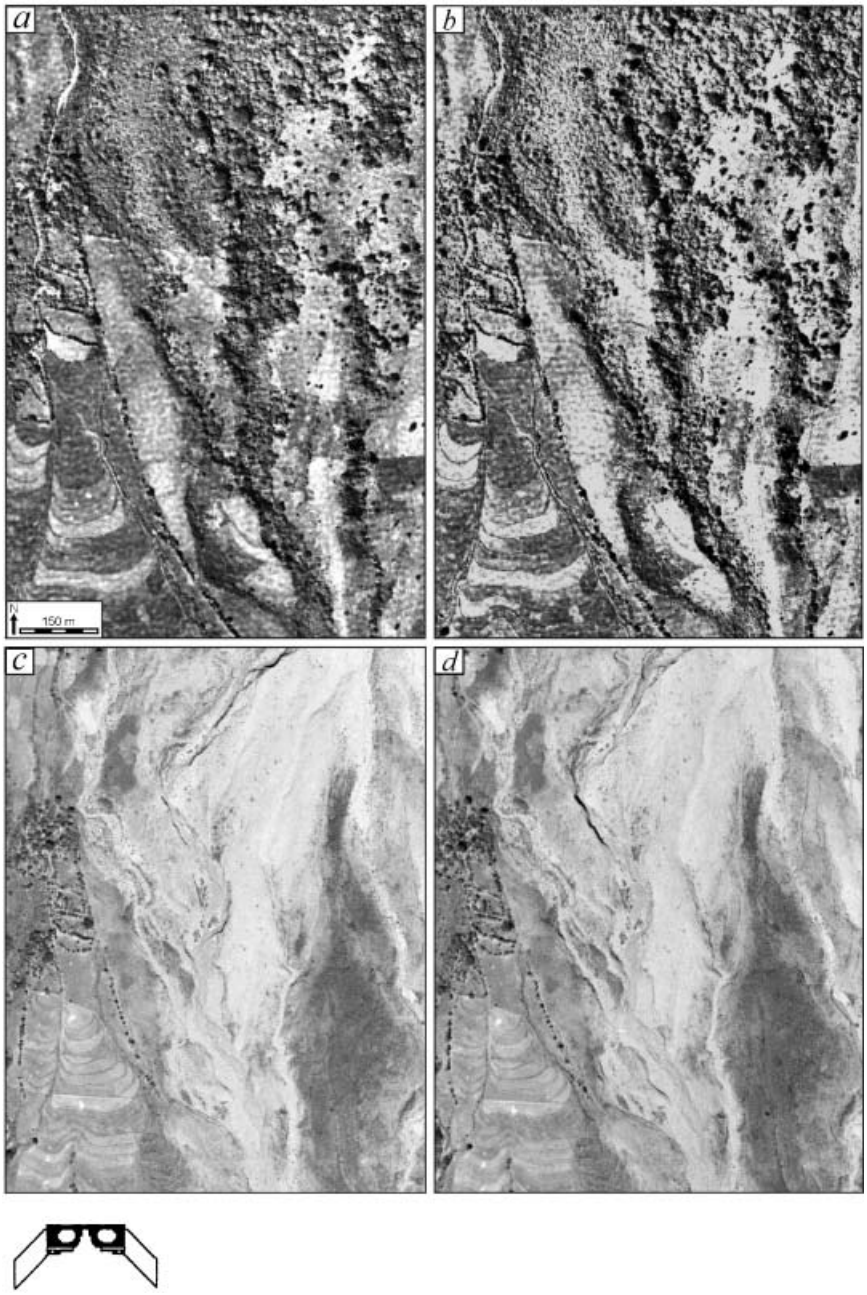

Figure 10. Stereograms of 1996 (*a* and *b*), and 2000 aerial photographs (*c* and *d*) of a drainage channel in the upper lahar deposition area (location indicated in figure 4(*b*), (*c*)). Note how the post-event channel system closely follows the pre-existing one. A detailed DEM-of-change revealed that no significant widening or change in depth occurred. The stereograms are best viewed with a standard pocket stereoscope.

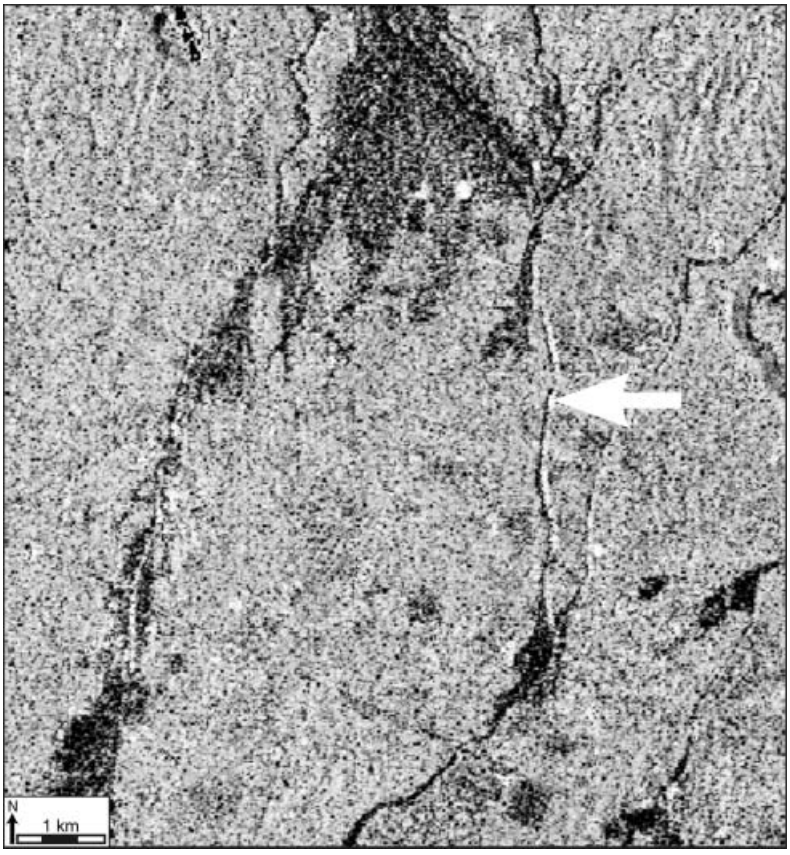

Figure 11. Merged image of post-event ERS SAR and SPOT XS, using IHS transformation. The SAR scene was integrated as intensity prior to reverse transform. Note the bright radar return along the eastern lahar runout flow, indicating a deep gully (arrow). Radar illumination is from the west.

Figure 12(*c*) shows the post-event SPOT image fused with a topographic map of the area, and draped over a DEM. The map shows clearly that actually two towns were affected. Also note how the main channel (as highlighted in figure 4(*c*)) corresponds to a pre-existing riverbed. The DEM (inset) is also able to resolve the ambiguity of flow origin mentioned in §6.2. The source is clearly not connected with the crater, discounting crater-lake breach, but rather with a steep flank. This also makes a dammed water body as the water source unlikely. ERS imagery revealed a lack of dammed water bodies within the flow area, which reduces the probability of further flows. However, having identified a steep flank as the source of the flow suggests a residual risk of further catastrophic failures, although with a likelihood decreasing with reduced precipitation, which triggered the original collapse.

It is important to stress that successful damage assessment strongly depends on the accuracy and comprehensiveness of the auxiliary data used. For example, the GIS database used here (compiled by the US Center for Integration of Natural Disaster Information (CINDI) following Mitch) still shows a railway line that was actually taken out of service in 1994. Several names of settlements close to the lahar are also incorrect, and no population data are included.

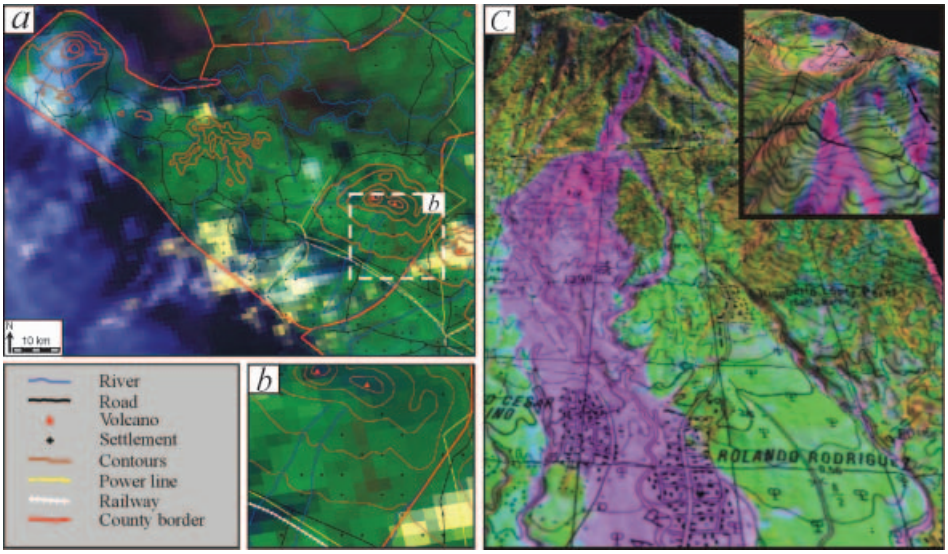

Figure 12. (*a*) AVHRR scene from 13 November 1998 within a GIS framework, showing the Casita lahar in relation to lifelines and other infrastructure (subset as (*b*)). (*c*) Post-event SPOT image of 25 November 1998, IHS-integrated with a topographic map, and draped over a DEM. The inset illustrates that the lahar originated as a flank collapse south–east of the Casita summit. See text for discussion.

9. Conclusions

The central aim of this study was a detailed characterization of the 1998 Casita lahar event, using a variety of remote sensing data types. The event was precipitation-triggered, and typical for both its tropical location and widespread, disastrous consequences. The interest in, but also the challenge of understanding, the event in detail is demonstrated by the number of on-site field campaigns that resulted, involving scientists from the USGS, the Czech Geological Survey, and universities in the US, the UK and Belgium. Given the time and cost involved in, as well as the limitations afforded by, fieldwork, remote sensing has evolved into a vital aid.

At Casita, the utility of remote sensing was found to be largely dependent on the questions asked, specifically on their time-criticality. The investigation of flow deposit structure and morphology is largely of scientific interest, and can draw on image information acquired some time after the event (under suitable circumstances). High spatial resolution optical images (SPOT) were found to be most appropriate to delineate the deposits and assess their structure and morphology, although the identification of damage, sedimentology, and flow transformation phases was limited. Low spatial resolution images (AVHRR) had the advantage of more frequent and extensive coverage, and cost-free, rapid availability. However, the poor spatial resolution and image distortion away from nadir greatly restrict the utility for comparatively small, Casita-type events. Both types of optical imagery suffered from clouds typical for volcanic structures in the tropics. SAR imagery, shown to be very useful in previous studies of (largely ash-derived) lahars, and valued for its cloud-penetrating abilities, essentially failed to see the flow deposition area. This was due to the short wavelength C-Band, relatively coarse flow deposits

derived from an initial debris avalanche and eroded colluvium, and dense wooden debris littering the area. RADARSAT, with its higher incident angle, was better suited for this rough surface than ERS. The radar data available here were most useful to identify a lack of persistent flooding, as well as lineaments and structures indicating a debris avalanche. The most useful aspects of remote sensing data were the availability of pre-event reference imagery, the synoptic coverage, the potential for quantitative work (e.g. as anaglyphs) when geo-registered or used with ground control points, and the complementary nature of different image types.

Used separately, however, all image types available showed limitations, related to spatial, spectral or radiometric sensor characteristics. Common to all is also their inability to reveal sub-surface information, for example that at least three lahars (of similar or larger size than the 1998 event) had descended the same flank vector in the last 8330 years (Scott *et al*., forthcoming). Koopmans and Forero (1993) used radar images to identify prehistoric lahars in Colombia based on smooth deposition fans, where deeply incised valleys, typical for the Southern Andes, meet the Magdalena Valley (see their figure 5). The lack of such channelled topography at Casita prevents such inferences.

The highest synergistic potential was not found, as in previous studies, in combining optical with radar, or high with low spatial resolution data, but in adding auxiliary information such as GIS, elevation or map data. In particular for disaster management questions (e.g. damage assessment), such increasingly available data are vital, as small features, such as utility and life-lines, but also political boundaries, are difficult or impossible to identify in images. Unfortunately, no suitable images were captured—by any non-classified satellite—in the critical hours after the event. At Casita, given the proximity to existing military infrastructure, an airborne survey would have been the most appropriate and useful approach.

Response to future lahar events will benefit from at least 20 new satellites slated for launch within the next 3 years. Among the more promising ones are Envisat's ASAR, PALSAR (onboard ALOS) and RADARSAT 2, all capable of like- and cross-polarization and variable incident angle acquisition, with RADARSAT providing very high (3 m) spatial resolution and 3-day revisits. PALSAR will also use the longer L-Band, overcoming some of the C-Band limitations discussed in this study. OrbView4 was expected to provide 8-m hyperspectral imagery (200 channels), particularly useful for material discrimination, for example to detect inter-lahar material variation, which can be linked to flow source and lahar transformations. Following failure of that satellite during launch in 2001, hyperspectral data are now available from the Hyperion sensor on NASA's EO-1. The first commercial hyperspectral satellite, ARIES-1, is scheduled for launch in 2005.

Acknowledgments

The ERS images were funded by the Centre de Recherches Volcanologiques (CRV). Access to two SPOT XS scenes, the panchromatic ortho-SPOT image, the RADARSAT image, and the 1996 aerial photos was provided by the Nicaraguan government (Instituto Nicaragüense de Estudios Territoriales (INETER)). The December 1998 aerial photos were obtained by the US Open Skies programme, and are available in the public domain, as are the CINDI GIS data and the AVHRR

images. Kerle also thanks INETER for valuable support during work in Nicaragua, Pedro 'El Caminante' Hernandez for assistance in the field, and Kevin Scott and James Brasington for helpful discussions. He would also like to thank the German Academic Exchange Service (DAAD), Cambridge University, and Sidney Sussex College for financial support.

References

ALEXANDER, D., 1991, Information technology in real-time for monitoring and managing natural disasters. *Progress in Physical Geography*, **15**, 238–260.

ARLENE, M., EVANGELISTA, M. A. M., REYES, P. J. D., SAITO, G., and IMAI, H., 1995, Application of satellite image-analysis for the estimation of Mt Pinatubo mudflow distribution. *Soil Science and Plant Nutrition*, **41**, 367–370.

BARRETO, P. E., 1998, Testimonios relacionados con los ruidos y imágenes fatales segundos antes de la tragedia, llegada repentinamente desde del volcán Casitas a las comunidades Rolando Rodriguez y El Porvenir. Instituto Nicaragüense de Estudios Territoriales, Managua, Nicaragua.

BIRK, R. J., MCCANDLESS, S. W., and SVEJKOVSKY, J., 1995, Disaster operations satellite system—an approach to applying remote sensing to disaster management. *3rd International Symposium on Spectral Sensing Research (ISSSR), 26 November–1 December 1995 (Melbourne, Australia)*. Available at: http://ltpwww.gsfc.nasa.gov/ISSR-95/disaster.htm

CARN, S. A., 1999, Application of synthetic aperture radar (SAR) imagery to volcano mapping in the humid tropics: a case study in East Java, Indonesia. *Bulletin of Volcanology*, **61**, 92–105.

CHAVEZ, P. S., SIDES, S. C., and ANDERSON, J. A., 1991, Comparison of 3 different methods to merge multiresolution and multispectral data—Landsat TM and SPOT panchromatic. *Photogrammetric Engineering and Remote Sensing*, **57**, 295–303.

CHOROWICZ, J., DEFFONTAINES, B., HUAMANRODRIGO, D., GUILLANDE, R., LEGUERN, F., and THOURET, J. C., 1992, SPOT satellite monitoring of the eruption of Nevado Sabancaya volcano (Southern Peru). *Remote Sensing of Environment*, **42**, 43–49.

CHOROWICZ, J., LOPEZ, E., GARCIA, F., PARROT, J. F., RUDANT, J. P., and VINLUAN, R., 1997, Keys to analyze active lahars from Pinatubo on SAR ERS imagery. *Remote Sensing of Environment*, **62**, 20–29.

DOBSON, M. C., ULABY, F. T., and PIERCE, L. E., 1995, Land-cover classification and estimation of terrain attributes using synthetic-aperture radar. *Remote Sensing of Environment*, **51**, 199–214.

FERRARO, R., VICENTE, G., BA, M., GRUBER, A., SCOFIELD, R., LI., Q., and WELDON, R., 1999, Satellite techniques yield insight into devastating rainfall from Hurricane Mitch. *EOS*, **80**, 505–514.

FRANCIS, P. W., 1994, The role of satellite remote sensing in volcanic hazard mitigation. Natural hazard assessment and mitigation: the unique role of remote sensing. The Royal Society, London, UK, pp. 17–21.

FRANCIS, P. W., and WELLS, G. L., 1988, Landsat Thematic Mapper observations of debris avalanche deposits in the central Andes. *Bulletin of Volcanology*, **50**, 258–278.

GARCIA, F., DELOS REYES, P., and CHOROWICZ, J., 1997, Comparison of SPOT and SAR ERS-1 data in mapping of volcanic deposits on the western flank of Pinatubo volcano. *The 3rd ERS symposium (Florence, Italy)*, ESA Publication SP-414, vol. 1, pp. 569–572.

GUO, H. D., LIAO, J. J., WANG, C. L., WANG, C., FARR, T. G., and EVANS, D. L., 1997, Use of multifrequency, multipolarization shuttle imaging radar for volcano mapping in the Kunlun Mountains of western China. *Remote Sensing of Environment*, **59**, 364–374.

HANKE, H. P., 1991, Bedarfsanalyse zur satellitengestützten Umweltüberwachung (BESU), FE-Vorhaben 1001 09001/01-02. Umweltbundesamt, Berlin.

HARRIS, J. R., MURRAY, R., and HIROSE, T., 1990, IHS transform for the integration of radar imagery with other remotely sensed data. *Photogrammetric Engineering and Remote Sensing*, **56**, 1631–1641.

IGLSEDER, H., ARENSFISCHER, W., and WOLFSBERGER, W., 1995, Small satellite constellations for disaster detection and monitoring. *Advances in Space Research*, **15**, 79–85.

JIANG, J., and CAO, S., 1994, Real-time disaster monitoring system by using SAR. *Microwave Instrumentation and Satellite Photogrammetry for Remote Sensing of the Earth, September 1994 (Rome, Italy)* (Bellingham,WA: International Society for Optical Engineering), pp. 91–97.

KERLE, N., 1996, Economic evaluation and human perspective for a moderate volcanic eruption at Arenal. *Boletín del Observatorio Vulcanológico del Arenal*, **6**, 53–70.

KERLE, N., 2002, Volume estimation of the 1998 flank collapse at Casita volcano, Nicaragua—a comparison of photogrammetric and conventional techniques. *Earth Surface Processes and Landforms*, **27**, 759–771.

KERLE, N., and OPPENHEIMER, C., 2002, Remote sensing as a tool in lahar disaster management. *Disasters*, **26**, 140–160.

KERLE, N., and VAN WYK DE VRIES, B., 2001, The 1998 debris avalanche at Casita volcano, Nicaragua—investigation of structural deformation as the cause of slope instability using remote sensing. *Journal of Volcanology and Geothermal Research*, **105**, 49–63.

KOOPMANS, B. N., and FORERO, G., 1993, Airborne SAR and Landsat MSS as complementary information source for geological hazard mapping. *ISPRS Journal of Photogrammetry and Remote Sensing*, **48**, 28–37.

KURODA, T., ORII, T., and KOIZUMI, S., 1997, Concept of Global Disaster Observation Satellite system (GDOS) and measures to be taken for its realization. *Acta Astronautica*, **41**, 537–549.

LI, J., 2000, Spatial quality evaluation of fusion of different resolution images. *International Archives of ISPRS Congress XIX, 16–23 July 2000, Amsterdam, The Netherlands* (Washington, DC: ISPRS), pp. 339–346.

LOPEZ, E. D., PARINGIT, E. C., and LIM, M. G., 1998a, Integration of ERS-1 SAR and Adeos AVNIR data to detect lahar damage extent in Pampanga Bay. *Euro-Asia Space Week 'Where East Meets West', 23–27 November 1998, Singapore* (Noordwijk: ESA), pp. 213–217.

LOPEZ, E. D., VINLUAN, R. J. N., and PARINGIT, E. C., 1998b, Lahar damage assessment using satellite remote sensing: the Mount Pinatubo experience. *International Symposium on Information Technology Tools for Natural Disaster Risk Management, 4–6 February 1998, Bangkok, Thailand* (Japan: University of Tokyo), pp. 175–182.

LUSCOMBE, B. W., and HASSAN, H. M., 1993, Applying remote sensing technologies to natural disaster risk management—implications for developmental investments. *Acta Astronautica*, **29**, 871–876.

MOLNIA, B. F., and HALLAM, C. A., 1999, Open Skies aerial photography of selected areas in Central America affected by Hurricane Mitch. US Department of the Interior; US Geological Survey, Washington.

MOUGINIS-MARK, P. J., 1995, Preliminary observations of volcanoes with the Sir-C radar. *IEEE Transactions on Geoscience and Remote Sensing*, **33**, 934–941.

PARESCHI, M. T., CAVARRA, L., FAVALLI, M., GIANNINI, F., and MERIGGI, A., 2000, GIS and volcanic risk management. *Natural Hazards*, **21**, 361–379.

POHL, C., and VAN GENDEREN, J. L., 1998, Multisensor image fusion in remote sensing: concepts, methods and applications. *International Journal of Remote Sensing*, **19**, 823–854.

RENGERS, N., SOETERS, R., and VAN WESTEN, C. J., 1992, Remote sensing and GIS applied to mountain hazard mapping. *Episodes*, **15**, 36–45.

RODOLFO, K. S., 2000, The hazard from lahars and jökulhlaups. In *Encyclopedia of Volcanoes*, edited by H. Sigurdsson (London: Academic Press), pp. 973–995.

SAN MIGUEL-AYANZ, J., VERSTRATETE, M. M., PINTY, B., MEYER-ROUX, J., and SCHMUCK, G., 2000, The use of existing and future remote sensing systems in natural hazard management: specifications and requirements. In *Observing Land From Space: Science, Customers and Technology*, edited by M. M. Verstratete, M. Menenti and J. Peltoniemi (Dordrecht: Kluwer Academic Publishers), pp. 53–60.

SHABAN, M. A., DIKSHIT, O., 2001, Improvement of classification in urban areas by the use of textural features: the case study of Lucknow city, Uttar Pradesh. *International Journal of Remote Sensing*, **22**, 565–593.

SHENG, Y. W., SU, Y. F., and XIAO, Q. G., 1998, Challenging the cloud-contamination

problem in flood monitoring with NOAA/AVHRR imagery. *Photogrammetric Engineering and Remote Sensing*, **64**, 191–198.

SHERIDAN, M. F., BONNARD, R., CARREÑO, R., SIEBE, C., STRAUCH, W., NAVARRO, M., CALERO, J. C., and TRUJILO, N. B., 1999, 30 October 1998 rock fall/avalanche and breakout flow of Casita volcano, Nicaragua, triggered by Hurricane Mitch. *Landslide News*, 2–4.

SHOWALTER, P. S., 2001, Remote sensing's use in disaster research: a review. *Disaster Prevention and Management*, **10**, 21–29.

SHOWALTER, P. S., and RAMSPOTT, M., 1999, The use of remote sensing in detecting and analysing natural hazards and disasters: a partially annotated bibliography. James and Marylin Lovell Center for Environmental Geography and Hazard Research, Department of Geography, Southwest Texas State University, San Marcos, TX.

SIEBERT, L., 1984, Large volcanic debris avalanches—characteristics of source areas, deposits, and associated eruptions. *Journal of Volcanology and Geothermal Research*, **22**, 163–197.

THOURET, J. C., LAVIGNE, F., KELFOUN, K., and BRONTO, S., 2000, Toward a revised hazard assessment at Merapi volcano, Central Java. *Journal of Volcanology and Geothermal Research* **100**, 479–502.

TOBIAS, A., LEIBRANDT, W., FUCHS, J., and EGURROLA, A., 2000, Small satellites: enabling operational disaster management systems. *Acta Astronautica*, **46**, 101–109.

TORRES, R., QUIAMBAO, R., MOUGINIS-MARK, P. J., GABRIEL, H., and SELF, K. K. S., 1999, Hazard monitoring at Pinatubo volcano using multi-temporal radar data. *Asian Conference on Remote Sensing, Hong Kong, China* (Joint Laboratory for Geo-Information Science of the Chinese Academy of Sciences and the Chinese University of Hong Kong), pp. 103–104.

UI, T., 1983, Volcanic dry avalanche deposits—identification and comparison with nonvolcanic debris stream Deposits. *Journal of Volcanology and Geothermal Research*, **18**, 135–150.

UI, T., TAKARADA, S., and YOSHIMOTO, M., 2000, Debris avalanches. In *Encyclopedia of Volcanoes*, edited by H. Sigurdsson (London: Academic Press), pp. 617–626.

VALLANCE, J. W., 2000, Lahars. In *Encyclopedia of Volcanoes*, edited by H. Sigurdsson (London: Academic Press), pp. 601–616.

VANDEMEULEBROUCK, J., THOURET, J. C., and DEDIEU, J. P., 1993, Identifying eruptive products and lahars by remote sensing of a SPOT image at and around the Nevado del Ruiz volcano, Colombia. *Bulletin de la Societe Geologique de France*, **164**, 795–806.

VENCATASAWMY, C. P., CLARK, C. D., and MARTIN, R. J., 1998, Landform and lineament mapping using radar remote sensing. In *Landform Monitoring, Modelling and Analysis*, edited by S. N. Lane, K. S. Richards and J. H. Chandler (Chichester: John Wiley & Sons), pp. 165–194.

WADGE, G., FRANCIS, P. W., and RAMIREZ, C. F., 1995, The Socompa collapse and avalanche event. *Journal of Volcanology and Geothermal Research*, **66**, 309–336.

WALTER, L. S., 1994, Natural hazard assessment and mitigation from space: the potential of remote sensing to meet operational requirements. Natural hazard assessment and mitigation: the unique role of remote sensing. The Royal Society, London, UK, pp. 7–12.

YATABE, S. M., and LECKIE, D. G., 1995, Clearcut and forest-type discrimination in satellite SAR imagery. *Canadian Journal of Remote Sensing*, **21**, 455–467.

ZHANG, Y., 1999, A new merging method and its spectral and spatial effects. *International Journal of Remote Sensing*, **20**, 2003–2014.

ZHOU, J., CIVCO, D. L., and SILANDER, J. A., 1998, A wavelet transform method to merge Landsat TM and SPOT panchromatic data. *International Journal of Remote Sensing*, **19**, 743–757.

ZIMMERMAN, P. D., 1991, The role of satellite remote sensing in disaster relief. *Space Communications*, **8**, 141–152.